ARTICLE

WILEY | BIOTECHNOLOGY BIOENGINEERING

Effects of scaffold microstructure and low intensity pulsed ultrasound on chondrogenic differentiation of human mesenchymal stem cells

Mitra Aliabouzar [ORCID] | Se-jun Lee | Xuan Zhou | Grace Lijjie Zhang | Kausik Sarkar

Department of Mechanical and Aerospace Engineering, The George Washington University, Washington DC

Correspondence
Kausik Sarkar, The George Washington University, 800 22nd Street NW, Suite 3000, Washington DC 20052.
Email: sarkar@gwu.edu

Funding information
George Washington University, Grant number: CDRF; National Science Foundation, Grant number: CBET-1205322

Abstract

The effects of low intensity pulsed ultrasound (LIPUS) on proliferation and chondrogenic differentiation of human mesenchymal stem cells (hMSCs) seeded on 3D printed poly-(ethylene glycol)-diacrylate (PEG-DA) scaffolds with varying pore geometries (square and hexagonal channels) were investigated. The scaffold with square pores resulted in higher hMSC growth and chondrogenic differentiation than a solid or a hexagonally porous scaffold. The optimal LIPUS parameters at 1.5 MHz were found to be 100 mW/cm^2 and 20% duty cycle. LIPUS stimulation increased proliferation by up to 60% after 24 hr. For chondrogenesis, we evaluated key cartilage biomarkers abundant in cartilage tissue; glycosaminoglycan (GAG), type II collagen and total collagen. LIPUS stimulation enhanced GAG synthesis up to 16% and 11% for scaffolds with square and hexagonal patterns, respectively, after 2 weeks. Additionally, type II collagen production increased by 60% and 40% for the same patterns, respectively under LIPUS stimulation after 3 weeks. These results suggest that LIPUS stimulation, which has already been approved by FDA for treatment of bone fracture, could be a highly efficient tool for tissue engineering in combination with 3D printing and hMSCs to regenerate damaged cartilage tissues.

KEYWORDS
3D printing, chondrogenesis, cartilage, LIPUS, tissue engineering, ultrasound

1 | INTRODUCTION

Over 6 million people visit the hospital due to cartilage injuries every year (Zhang, Hu, & Athanasiou, 2009; Zhou et al., 2017). Cartilage injury leads to arthritis, which involves erosion of the articulating surfaces of joints, and is the most common disabling human condition affecting 33.6 % of adults aged 65 and older in the U.S (Kuo, Li, Mauck, & Tuan, 2006; Lawrence et al., 2008). Cartilage is an avascular tissue notorious for its complex stratified structure as well as very low capacity of self-repair after injury (Buckwalter & Mankin, 1997; Zhang et al., 2009). Existing methods of treatment, such as allografts, autografts, and total joint replacement, have their associated shortcomings and complications including donor site morbidity, insufficient donor tissues and infection (Clair, Johnson, & Howard, 2009; Temenoff & Mikos, 2000). Nearly, 11% of patients with hip replacements and 8% of those with knee replacement had revision operations in 2003 in the U.S. due to failed implant surgeries (Andersson, 2008).

Tissue engineering offers novel approaches towards repairing or replacing damaged tissues for the purpose of restoring tissue functionality. Effective tissue regeneration requires a viable cell source, a biocompatible scaffold, suitable growth factors and mechanical cues (Kassem, 2004). Chondrocytes, which reside in the cartilage tissue, are the most obvious candidate for cartilage regeneration. However, they are limited in number and tend to lose their phenotype after multiple expansions in culture (Finger et al., 2004). Human mesenchymal stem cells (hMSCs) are a promising cell source for facilitating tissue repair due to their abundance and ability to differentiate into many cell types such as osteoblasts, chondrocytes, adipocytes, and myocytes given the appropriate conditions (Johnstone, Hering, Caplan, Goldberg, & Yoo, 1998; Pittenger et al., 1999).

Ultrasound (US) is widely used for diagnostic purposes. It also offers a convenient means for transferring mechanical energy into biological tissues (Williams, 1983). However clinical utilization of low intensity ultrasound (intensities lower than 1 W/cm^2) has been so far limited to bone fracture healing (Azuma et al., 2001; Heckman, Ryaby, McCabe, Frey, & Kilcoyne, 1994). Low intensity pulsed ultrasound (LIPUS) has been well documented to have various therapeutic effects on cells and enhance bone formation in vitro and in vivo (Parvizi, Wu, Lewallen, Greenleaf, & Bolander, 1999; Takayama et al., 2007; Zhang, Huckle, Francomano, & Spencer, 2003). Previous studies investigated the beneficial effects of LIPUS on proliferation of fibroblasts, osteoblasts, and chondrocytes (Doan, Reher, Meghji, & Harris, 1999; Harle, Salih, Mayia, Knowles, & Olsen, 2001; Nishikori et al., 2002). Enhanced gene expression (Choi, Woo, Min, & Park, 2006), type II collagen (Korstjens, Van der Rijt, Albers, Semeins, & Klein-Nulend, 2008; Mukai et al., 2005), glycosaminoglycan (GAG) synthesis (Ebisawa et al., 2004), collagen and protein syntheses (Saito, Fujii, Tanaka, & Soshi, 2004), calcium deposition (Zhou, Castro, et al., 2016) and bone morphogenetic protein-2 (Suzuki et al., 2009) have been reported in the literature as positive impacts of LIPUS.

The above mentioned experiments were almost exclusively conducted on monolayer cell cultures (2D) or thin film hydrogels, which are very different from the complex physiological environment that cells find inside the body. Three dimensional (3D) tissue scaffolds can provide suitable microenvironment better representing the actual in vivo situation. An ideal tissue engineering scaffold should be biocompatible, promote cell growth, have suitable porosity to allow cell migration as well as nutrients exchange and finally provide satisfactory mechanical properties (Athanasiou, Darling, & Hu, 2009). 3D printing techniques hold great promise for better design and control of scaffolds' structure and properties which result in reproducible and precise microstructures with patient-specific geometry (Castro, O'Brien, & Zhang, 2015; Zhou, Zhu, et al., 2016).

The literature on the effects of LIPUS on differentiation of hMSCs on 3D scaffolds is sparse (Aliabouzar, Zhang, & Sarkar, 2016; Lai et al., 2010; Zhou et al., 2017). Cui and coworkers found that rabbit MSCs seeded on non-porous poly-glycolic acid (PGA) produced significantly more chondrogenic biomarkers when treated with 200 mW/cm^2 LIPUS (Cu, Park, Park, & Min, 2006; Cui et al., 2007). Hsu, Kuo, Whu, Lin, and Tsai (2006) reported positive effects of ultrasound on neocartilage formation in the human chondrocytes seeded on composite scaffolds.

Recently, we investigated the effects of lipid-coated-microbubble-assisted ultrasound stimulation on chondrogenesis of hMSCs (Aliabouzar et al., 2016). It is however important to investigate effects of each individual component of the mechanical cues and environment —LIPUS, microbubbles, scaffold structure—in promoting the phenomenon. Specifically, cellular behavior is directly affected by scaffold architecture (porosity, pore size, and interconnectivity) (Sobral, Caridade, Sousa, Mano, & Reis, 2011; Zeltinger, Sherwood, Graham, Müeller, & Griffith, 2001). Here, we investigate the effects of LIPUS on hMSC proliferation and chondrogenic differentiation in 3D scaffolds of varying pore geometry—solid, square and hexagonal. We fabricated scaffolds from poly-(ethylene glycol)-diacrylate (PEG-DA) printed by a novel tabletop stereolithography-based technique developed in our lab (Aliabouzar et al., 2016; Zhu, O'Brien, O'Brien, & Zhang, 2014). PEG-DA, as a UV photocurable bioink, is chosen for its high water content (similar to cartilage composition), biocompatibility and easy printability (O'Brien, Holmes, Faucett, & Zhang, 2014). We have thoroughly evaluated the 1 and 3-day proliferation as well as 3-week chondrogenic differentiation of hMSCs seeded on 3D printed scaffolds with varying pore channels under optimized LIPUS treatment.

2 | MATERIALS AND METHODS

2.1 | Preparation of 3D-printed scaffolds

A tabletop stereolithography (SL)-based 3D bioprinter was used to fabricate porous scaffolds. SL is a 3D printing technique which uses light to cross link polymeric resins. The printer consists of a 3D axial movable stage and a UV laser source (Zhou, Castro, et al., 2016; Zhou et al., 2017; Zhou, Zhu, et al., 2016). An open source software (Prontrface) was employed to control the printing configuration. It can generate different geometrical patterns (e.g., square and hexagonal) using 3D computer aided design (CAD) models. The print speed was maintained at 25 mm/s and the laser repetition rate used to print the structured patterns varied from 8 to 11 kHz. The 3D scaffold was printed via a layer-by-layer method. We prepared two different porous scaffold geometries with square and hexagonal pores. A nonporous scaffold of the same material and dimension was prepared as the reference via direct UV crosslinking. The bioink was prepared by mixing 40% (w/w) poly (ethylene glycol) (PEG, Mn 300) and 60% (w/w) poly (ethylene glycol) diacrylate (PEG-DA, Mn 575) in the presence of the photo initiator (0.5% (w/w) of PEG-DA) (Holmes, Castro, Li, Keidar, & Zhang, 2013; Zhu, Holmes, Glazer, & Zhang, 2016).

2.2 | Characterization of scaffolds

The morphology of the scaffolds was observed by a scanning electron microscope (SEM, Zeiss NVision 40FIB). The compressive elastic modulus of the 3D printed scaffolds was determined via compression testing (n = 6) (Applied Test Systems, Butler, PA) fitted with a 100 N load cell at a crosshead speed of 0.5 mm/min. Samples were punched

by a 12-mm biopsy punch (Figure 3a) and were placed in ultrapure water overnight prior to testing. We plotted the stress-strain curves and calculated the Young's modulus from the linear region.

2.3 | In vitro cell culture

Primary hMSCs were purchased from the Texas A&M Health Science Center Institute for Regenerative Medicine. hMSCs (passage #3-6) were cultured in complete media composed of Alpha Minimum Essential medium (α-MEM) (Gibco, Grand Island, NY) supplemented with fetal bovine serum (FBS) (16%, v/v) (Atlanta Biologicals, Lawrenceville, GA), L-glutamine (1% v/v) (Invitrogen, Carlsbad, CA), and penicillin:streptomycin (1% v/v) (Invitrogen, Carlsbad, CA). Cells were incubated under standard cell culture conditions (37°C, 5% CO_2 and 95% relative humidity). For chondrogenesis, 100 nM dexamethasone, 40 µg/ml proline, 100 µg/ml sodium pyruvate, 50 mg/ml L-ascorbic acid 2-phosphate, and 1% ITS (1.0 mg/ml recombinant human insulin, 0.55 mg/ml human transferrin (substantially iron-free), and 0.5 µg/ml sodium selenite) were added to the above complete media. Media were replaced every other day. Printed slabs of scaffolds were punched into uniform and cylindrical scaffolds using a 12 mm biopsy punch prior to cell seeding (Figure 3a), the punched scaffolds were sterilized via UV exposure, immersed in 75% ethanol for 2 hr and then rinsed with PBS three times. Subsequently, the sterilized samples were pre-soaked in culture media for 24 hr before cell seeding. hMSCs were seeded at a density of 2×10^4 per scaffold in 24-well plates in complete media overnight before LIPUS experiments to permit complete cell attachment. On the following day, the media were replaced to remove non-adherent cells.

2.4 | Ultrasound excitation

The schematic representation of ultrasound exposure setup is shown in Figure 1. Briefly, the ultrasound pulse was produced by a programmable function generator (33250A, Agilent, Palo Alto, CA), amplified by a broadband 55 dB laboratory RF power amplifier (model A-150, ENI, Rochester, NY) and then emitted from a single element unfocused immersion transducer. The element diameter of the transducer (Olympus NDT, Waltham, MA), with central frequency of 2.25 MHz (−6 dB: 1.48–2.90 MHz), was 12.7 mm. The transducer was calibrated using a 0.4 mm needle hydrophone (HNC400, ONDA, Sunnyvale, CA) in a water tank filled with degassed deionized water. According to the transducer technical notes (Olympus, 2006) and our calculations, the near-field distance of an unfocused immersion transducer is 40.3 mm at 1.5 MHz, indicating that the cells are in the near-field distance as in many other investigations (Doan et al., 1999; Li, Chang, Lin, & Sun, 2002; Suzuki et al., 2009). However, this particular setup has the advantage of direct stimulation by the immersed transducer. Note that several animal and clinical trials of therapeutic ultrasound involved near-field stimulation by transducers in direct contact with the skin (Gebauer, Mayr, Orthner, & Ryaby, 2005; Heckman et al., 1994; Mayr, Frankel, & Rüter, 2000). Also note that Li et al. (2002) found the optimum intensity of US stimulation in a

far-field setup (exposure distance of 240 mm) to be identical to that found in a near-field setup (5 mm) by Parvizi et al. (1999).

To conduct this study, the transducer and the XYZ positioning stage (Newport Corp., CA) were sterilized with 75% ethanol and kept under ultraviolet light overnight before the experiments. The transducer head was placed vertically on the top of the culture plate until it touched the surface of the cell culture medium. In this configuration, the working distance of approximately 13 mm from the cell culture surface was fixed and kept constant throughout all experiments. Prior to ultrasound exposure the cells were carefully washed with PBS. Ultrasound was applied to the cells after adding 3.5 ml of medium to each well to fill the well completely (to prevent creating any trapped air bubbles). Control groups underwent the same submersion and withdrawal of transducers with ultrasound power turned off. To prevent the possibility of indirect-transfer of mechanical energy of US to the neighboring wells, hMSC-seeded scaffolds were distributed in every other well of a 24-well plate (one empty well in between) as shown in Figure 1a. The 24-well plates were placed in a water container (Figure 1b) to offer a water-polystyrene interface to the ultrasound instead of an air-polystyrene interface; the latter has a higher reflection coefficient than the former. All LIPUS stimulations were carried out at a constant pulse length of 200 µs, varying the duty cycle (20%, 25%, 50%, 80%, and continuous mode) and the excitation intensity (spatial average temporal average (SATA) of 30, 70, 100, 150, and 200 mW/cm2) to determine the optimum acoustic setting. The corresponding area averaged peak negative pressure at those SATA intensities are 61.46 kPa, 93.88 kPa, 112.21 kPa, 137.43 kPa, and 158.69 kPa. Note that duty cycle is the fraction of the time within a burst/pulse repetition period (PRP) the transducer is transmitting (pulse length/PRP); it was varied by changing the pulse repetition period. Samples were treated with varying LIPUS parameters for 3 min at the excitation frequency of 1.5 MHz.

2.5 | Determination of hMSC proliferation on 3D-printed scaffolds under LIPUS treatment

After LIPUS treatment for predetermined periods, cells were rinsed using phosphate buffer saline (PBS) and then lifted enzymatically with 0.25% trypsin-EDTA solution (Sigma Aldrich, St.Louis, MO). Cell proliferation was quantified via CellTiter 96 Aqueous Solution Cell Proliferation assay (MTS) (Promega, Madison, WI) and analyzed using a spectrophotometer (Thermo Fisher Scientific, Hudson, NH) at 490 nm (Katiyar, Duncan, & Sarkar, 2014) (Castro, Patel, & Zhang, 2015). MTS uses a colorimetric method to quantify viable cells. Only the metabolically active cells will absorb MTS tetrazolium compound and generate a colored formazan product. This formazan dye produced by viable cells can be quantified by measuring the absorbance at 490–500 nm using a spectrophotometer.

2.6 | Confocal microscopy of hMSC morphology after LIPUS treatment

Optical microscopy (AmScope FMA050, MA at 10×) was used to examine hMSC morphology on non-porous and porous scaffolds with
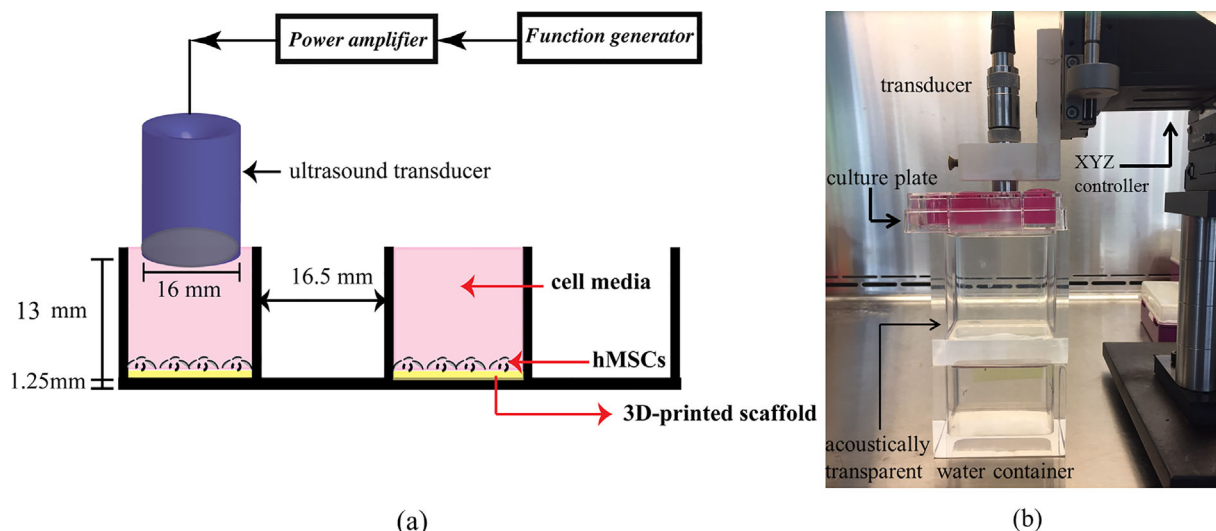
FIGURE 1   (a) Schematic illustration of the US exposure setup with dimensions of the transducer as well as the polystyrene 24-well plates, (b) customized experimental setup for LIPUS stimulation

square pore geometry prior to LIPUS treatment. For qualitative cell proliferation and growth, laser confocal microscopy (Carl Zeiss LSM 710) was used to visually assess cell performance on 3D-printed scaffolds before and after LIPUS stimulation. For confocal microscopy, all scaffolds were washed two times with PBS and fixed with 10% Formalin for 10 min followed by permeabilization in 0.1% Triton-100 for 10 min. hMSCs were double-stained with Texas red for 1 hr, and 4′,6-diamidino-2-phenylindole (DAPI) for 3 min. Scaffolds were then imaged at 20× magnification.

2.7 | Determination of hMSC chondrogenic differentiation on 3D-printed scaffolds under LIPUS treatment

All scaffolds for differentiation studies were seeded at a density of 1×10^5 cells per scaffold in chondrogenic media. After predetermined time periods of LIPUS treatments, these samples were collected after 1, 2, and 3 weeks to evaluate hMSC chondrogenesis. Media were removed from the samples and later rinsed with PBS. The collected samples were freeze dried in a lyophilizer for 48 hr and then treated in a papain-based enzymatic digestion solution for 18 hr in a 60°C water bath. Glycosaminoglycan (GAG), total collagen and collagen type II, key components of cartilage extracellular matrix (ECM), were evaluated using standard chondrogenic biochemistry assay kits following manufacturer's instructions similar to our previous studies (Castro, O'Brien, et al., 2015; Holmes, Zhu, Li, Lee, & Zhang, 2014; Zhou et al., 2017).

2.8 | Statistical analysis

All proliferation studies were run in triplicate. And then they were repeated three times in different days to further allow for day-to-day and donor variations leading to $n = 9$. For the chondrogenic differentiation studies, five replicates were performed ($n = 5$). Data

are presented as mean ± standard error of the mean (StdEM) and analyzed by the Student's t-test. A $p < 0.05$ was considered as statistically significant.

3 | RESULTS AND DISCUSSION

3.1 | Acoustic characterization of US stimulation setup

As noted above, the cells experience LIPUS stimulation in the non-uniform near-field. It was therefore felt important to characterize it. The acoustic output pressure of the transducer was calibrated at 1.5 MHz, 30 mW/cm2 pulse length of 200 μs and PRP of 1 ms using a needle hydrophone. The output pressure amplitude varies along the central axis with distance from the transducer head surface (Figure 2a). The arrow indicates the working distance of 13 mm used here for the LIPUS treatments of cells. Figure 2b shows the radial variation of the pressure amplitude field at axial distances of 13 mm and 58 mm (far-field) from the transducer face. However, presence of the cell well enclosure may result in a complex acoustic pressure field different from the free field due to reflection and standing waves. At the same time, the setup geometry (Figure 1) made the pressure field inside the cell well, with the transducer inserted, inaccessible to direct measurement. Instead, the pressure field just outside and near the well bottom, after its transmission through the bottom wall, was measured. The radial variations (Figure 2c) of the pressure at 13 mm with and without the well placed in the path of LIPUS were found to be similar, indicating a small reflection loss at the well bottom, and therefore possibly minimal standing wave effects. Note that we avoided strong reflections due to the large acoustic impedance mismatch at the air-polystyrene interface (specific acoustic impedance for air 426 kg/m²s; and polystyrene 2.5×10^6 kg/m²s) by placing the cell plates in a water (specific acoustic impedance 1.46×10^6 kg/m²s) container (Hensel, Mienkina, & Schmitz, 2011).
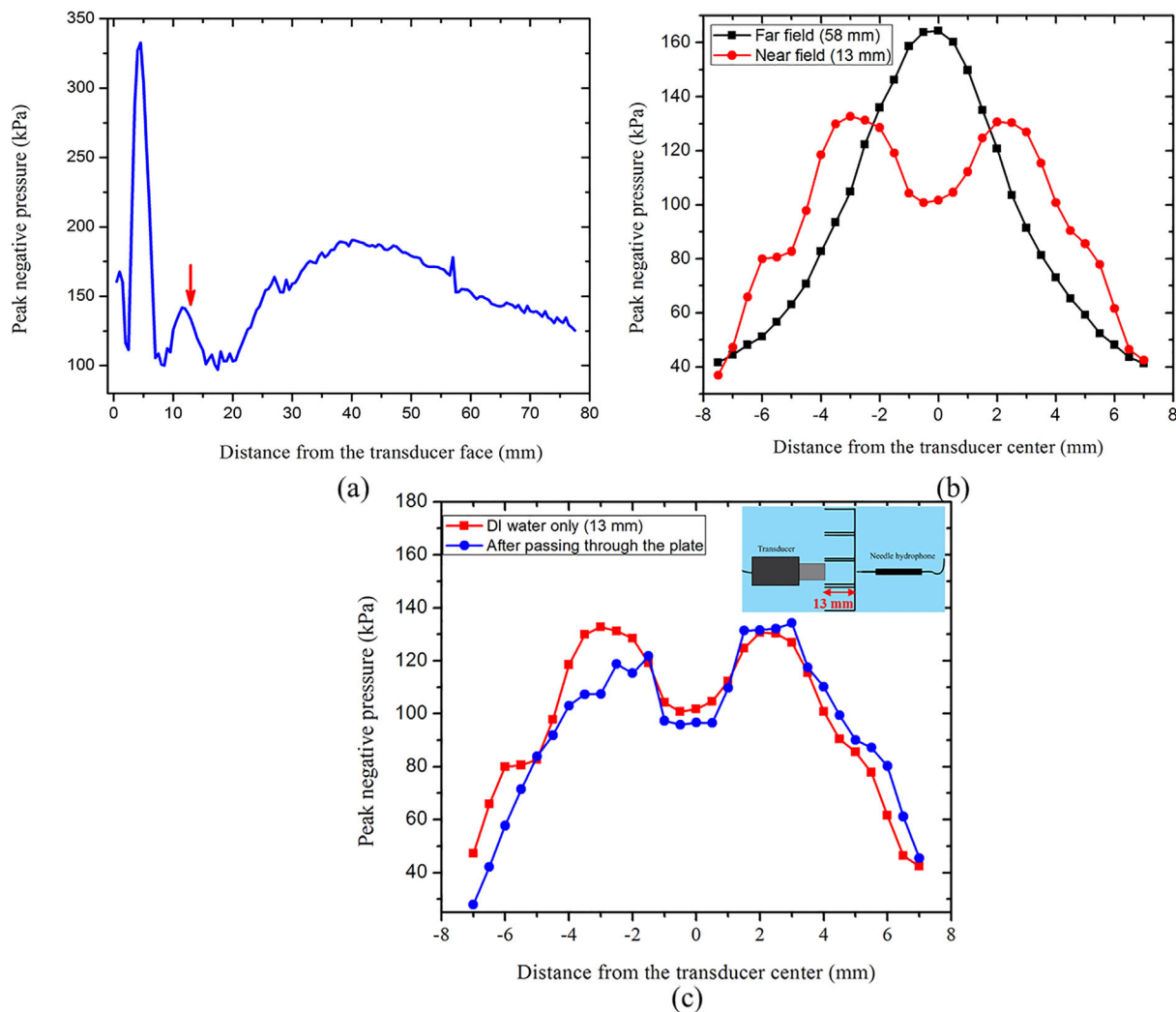
FIGURE 2 (a) Measured peak negative pressure along the axis of the transducer transmitting at 1.5 MHz and 30 mW/cm² through degassed distilled water, (b) Radial distribution of peak negative pressure at distances of 13 mm and 58 mm from the transducer surface, (c) Radial distributions of peak negative pressure at 13 mm with and without the wall of the cell culture plate

3.2 | Characterization of 3D-printed PEG-DA scaffolds

A scanning electron microscope (SEM, Zeiss NVision 40FIB) was employed to assess the matrix morphology and pore dimensions. Typical SEM images of 3D-printed porous scaffolds are presented in Figures 3b and 3c. 3D printed hydrogel scaffolds are highly porous with open and interconnected pores that are surrounded by polymer walls. As shown in the figure, the pores and channels in the 3D-printed scaffolds are distinct and have corresponded well to the pre-designed shapes. We calculated the porosity by measuring its solid phase density as well as apparent mass density according to (Kumar et al., 2016). All the measurements were repeated six times from different positions of the printed scaffolds. The scaffolds with square and hexagonal pore geometries had porosities of 49% and 33%, respectively. Using the image J software (imagej.nih.gov), the SEM images were analyzed to determine the average size of the pores. The pore dimension for the square and hexagonal shapes was found to be 700×690 and $760 \times 1130 \, \mu m^2$, respectively.

We plotted the stress-strain curves for the porous and non-porous hydrogel scaffolds, and calculated Young's modulus from the linear region. As shown in Figure 4, the non-porous hydrogel scaffold has the highest Young's modulus and it decreases as porosity increases (from 33% for a hexagonal scaffold to 49% for a square one), as can be expected (Hunger, Donius, & Wegst, 2013). All the scaffolds showed satisfactory mechanical properties similar to cartilage (0.75–1 MPa) and subchondral bone in human osteochondral tissue.

3.3 | Effects of LIPUS parameters on hMSC proliferation

The optimal LIPUS excitation intensity was determined by evaluating hMSC proliferation under various intensities (30, 70, 100, 150, and 200 mW/cm²). Other acoustic parameters (1.5 MHz, 20% duty cycle, 200 μs pulse length and 3-min excitation period) were kept constant. Twenty-four hours after LIPUS stimulation, proliferation of hMSC, seeded on scaffolds with square channels, was quantified using MTS
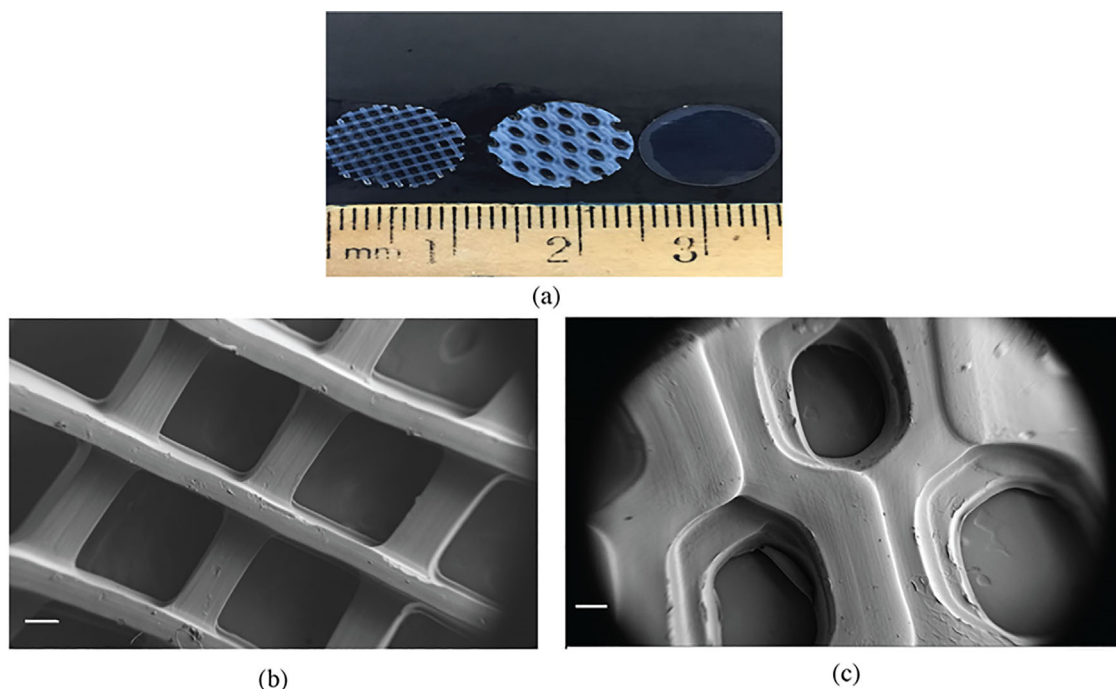
FIGURE 3 (a) Punched hydrogel scaffolds for cell studies using a 12 mm biopsy punch. Scanning electron microscopy images of 3D-printed scaffolds with (b) square and (c) hexagonal pore shapes. The bar shows 200 μm

assay. As demonstrated in Figure 5, excitation intensities of 70 and 100 mW/cm^2 enhanced hMSC growth by 15 % and 55 %, respectively, when compared to the control group (sham US). Higher intensities showed rather adverse effects. A low intensity of LIPUS may not induce sufficient mechanical stimulation for cell proliferation; while a high intensity of ultrasound may result in higher shear stresses disrupting the cell membrane (Dunn, 1985).The optimal intensity was kept constant at 100 mW/cm^2 for the rest of the studies. In our previous studies in presence of contrast microbubbles the optimum intensity was found lower, 30 mW /cm^2 (Aliabouzar et al., 2016).
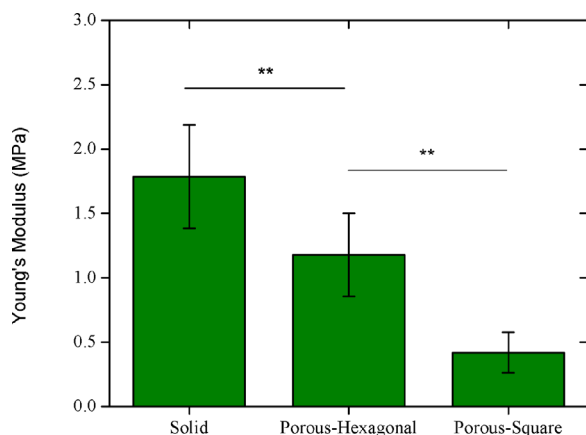
We investigated the effects of duty cycle in the range of 20–80% (i.e., pulse repetition period (PRP) in the range of 250 μs to 1 ms) as well as the continuous mode. We conducted the duty cycle study on hMSCs seeded on PEG-DA scaffolds with both square and hexagonal pore geometries. hMSC proliferation, 24 hr after LIPUS stimulation, was examined at varying duty cycles and the results are presented in Figure 6. The duty cycle of 20% (PRP of 1 ms) has induced the highest proliferation rates on both scaffolds (12% on hexagonal and 60% on square compared to control).

We note that similar experiments performed in monolayer 2D cell culture obtained different, albeit preliminary, values (unpublished) for optimum intensity (150 mW/cm^2) and duty cycle (50%) for maximum hMSC proliferation. It indicated the stark difference of LIPUS effects in two different environments and potential limitations of 2D cell culture studies. We use PRP of 1 ms (duty cycle of 20%) for all subsequent experiments.

3.4 | Effects of LIPUS on hMSC proliferation on scaffolds with different pore geometries

For 1 and 3-day proliferation studies with LIPUS excitation (at 100 mW/cm ^{2}, 1.5 MHz, duty cycle 20% and 200 μs pulse length), we divided our samples into three groups: (i) cells seeded on a non-porous solid PEG-DA as a reference, cells seeded on 3D-printed PEG-DA scaffolds with (ii) hexagonal and (iii) square patterns. At predetermined time points, the cell viability was measured by MTS assay with the results shown in Figure 7. The results indicate that hMSCs grow well on porous PEG-DA scaffolds with both pore
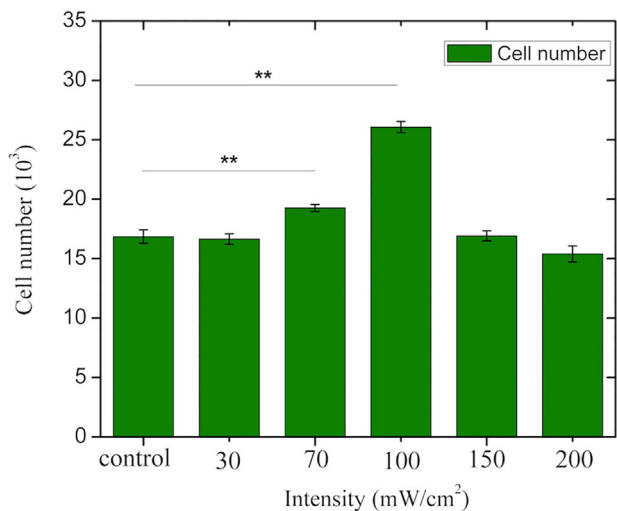

FIGURE 4 Compressive Young's modulus data for the solid and 3D printed scaffolds with varying pore geometry. Data are ± standard error, $n = 6$

FIGURE 5 Effects of 3-min LIPUS (1.5 MHz; 20% duty cycle; 200 µs pulse length) stimulation at varying intensities on hMSC proliferation after 24 hr (Data are mean ± StdEM, $n = 9$). Values significantly different from the control group are indicated by * for $p < 0.05$ and ** for $p < 0.01$

et al., 2005; Jin et al., 2000; Knychala et al., 2013; Rumpler, Woesz, Dunlop, van Dongen, & Fratzl, 2008; Zhou, Castro, et al., 2016). Nelson et al. (2005) correlated the curvature driven growth to regions of higher force concentrations. Note that the higher porosity rate (49% for square pores compared to 33% for hexagonal pores) and thereby better cell migration as well as facilitated transport of nutrients and oxygen could also contribute to the higher proliferation in the scaffolds with square pores. However, note that Zhou, Zhu, et al. (2016) found that a scaffold with square pores led to a higher cell proliferation than a scaffold with hexagonal pores even when the former is less porous than the latter. In addition, LIPUS stimulation significantly increased cell proliferation compared to the controls (Figure 7): 12% after 3 days of treatment in 3D printed scaffolds with square channels while 2.3% in the nonporous scaffold. An understanding of the impact of pore geometry as well as porosity on cellular behaviors and subsequently tissue formation could assist in developing suitable porous scaffolds for tissue engineering applications. Due to the limitation of our current 3D-printer, we could only study PEG-DA scaffolds with square and hexagonal channels. Future work will be directed to include more complex hierarchical geometries and varying porosities that better differentiate the effect of each.

hMSC morphology was evaluated using optical microscopy (Figures 8a and 8b). After 10 days of culture on non-porous PEGDA scaffolds, cells remained well attached. However, higher spreading and growth of hMSCs displayed in Figure 8b supports the ability of cells to grow upon and within the porous scaffolds with square pore geometry. Cell viability and proliferation before and after LIPUS was further assessed using confocal microscopy (Figure 8c–f). LIPUS stimulation enhanced cell growth in Figures 8d and 8f on square and hexagonal pores, respectively, compared to the experiments without LIPUS (Figures 8c and 8e).
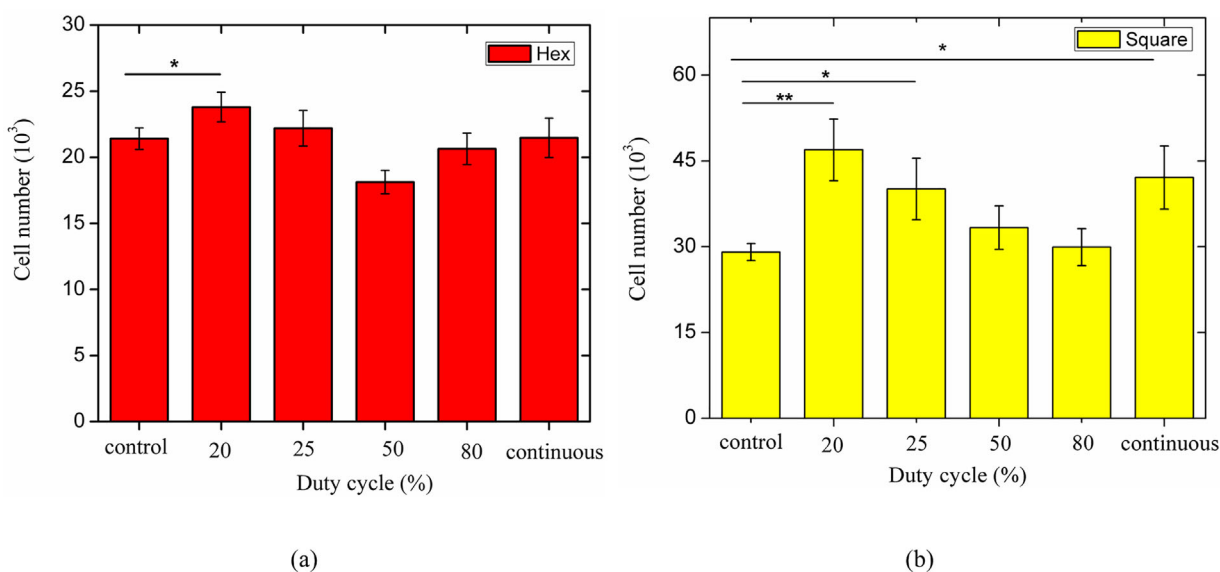
shapes when compared to the solid nonporous scaffolds. Porosity plays a key role in tissue-engineering applications since it provides a suitable environment for cells to grow and facilitate nutrient and oxygen diffusion as well as waste removal (Loh & Choong, 2013). Here we observed that square pore shape has exhibited a significantly higher proliferation rate compared to the hexagonal one. This could be attributed to the higher curvature of the square pores. Previous studies have indicated that MSCs preferentially adhere to corners and grow faster on larger curvatures (Habibovic

(a)

(b)

FIGURE 6 Effects of 3-min LIPUS (1.5 MHz; 100 mW/cm², 200 µs pulse length) stimulation at varying duty cycles on hMSC proliferation on scaffolds with (a) hexagonal and (b) square pore geometries after 24 hr (Data are mean ± StdEM, $n = 9$). Values significantly different from the control group are indicated by * for $p < 0.05$ and ** for $p < 0.01$
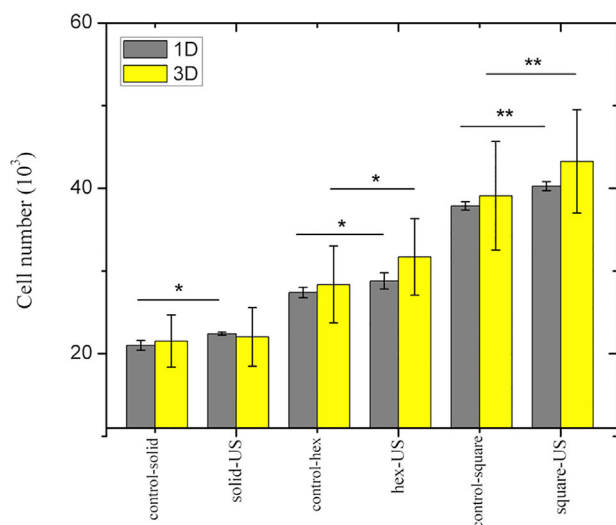
FIGURE 7 1 and 3-day hMSC proliferation with 3-min LIPUS (100 mW/cm2; 1.5 MHz; 20% duty cycle; 200 μs pulse length) (Data are mean ± StdEM, n = 9). Values significantly different from the control group are indicated by * for $p < 0.05$ and ** for $p < 0.01$

3.5 | Effects of LIPUS on hMSC chondrogenic differentiation on 3D-printed scaffolds

Proteoglycan and type II collagen are two major constituents of the extracellular matrix (ECM) of cartilage tissue, contributing to compressive and tensile properties of cartilage tissue, respectively (Hollander et al., 1995; Responte, Natoli, & Athanasiou, 2007). Seeded 3D-printed PEGDA scaffolds were evaluated for glycosaminoglycan (GAG), total collagen and type II collagen after three weeks of culture. As demonstrated in Figure 9, LIPUS treatment promoted GAG synthesis up to 16% and 11% for the scaffolds with square and hexagonal patterns, respectively, after 3 weeks compared to their controls. Similarly, total collagen synthesis increased up to 23% for hMSCs seeded on both 3D printed porous scaffolds after 3 weeks. The type II collagen synthesis was also significantly enhanced by LIPUS stimulation after 3 weeks (60% for scaffolds with square patterns and 40% for those with hexagonal).

Despite plethora of studies on positive effects of LIPUS on cells, the exact mechanism is not completely known. Several in vitro studies have reported that mechanical stimuli can activate distinct regulatory pathways, which in turn result in changes in matrix and collagen syntheses and metabolic functions of the cells (Grodzinsky, Levenston, Jin, & Frank, 2000; Kim, Grodzinsky, & Plaas, 1996; Sims, Karp, & Ingber, 1992). Other studies suggest that application of mechanical forces to integrins can activate mechanosensitive ion channels and trigger calcium entry into cells which may influence cell mechanics by modulating cytoskeletal structure or contractility (Matthews, Overby, Mannix, & Ingber, 2006; Munevar, Wang, & Dembo, 2004). Note that unlike steady mechanical stimulation as in tension, compression or fluid shear studied in the past (Buschmann, Gluzband, Grodzinsky, &
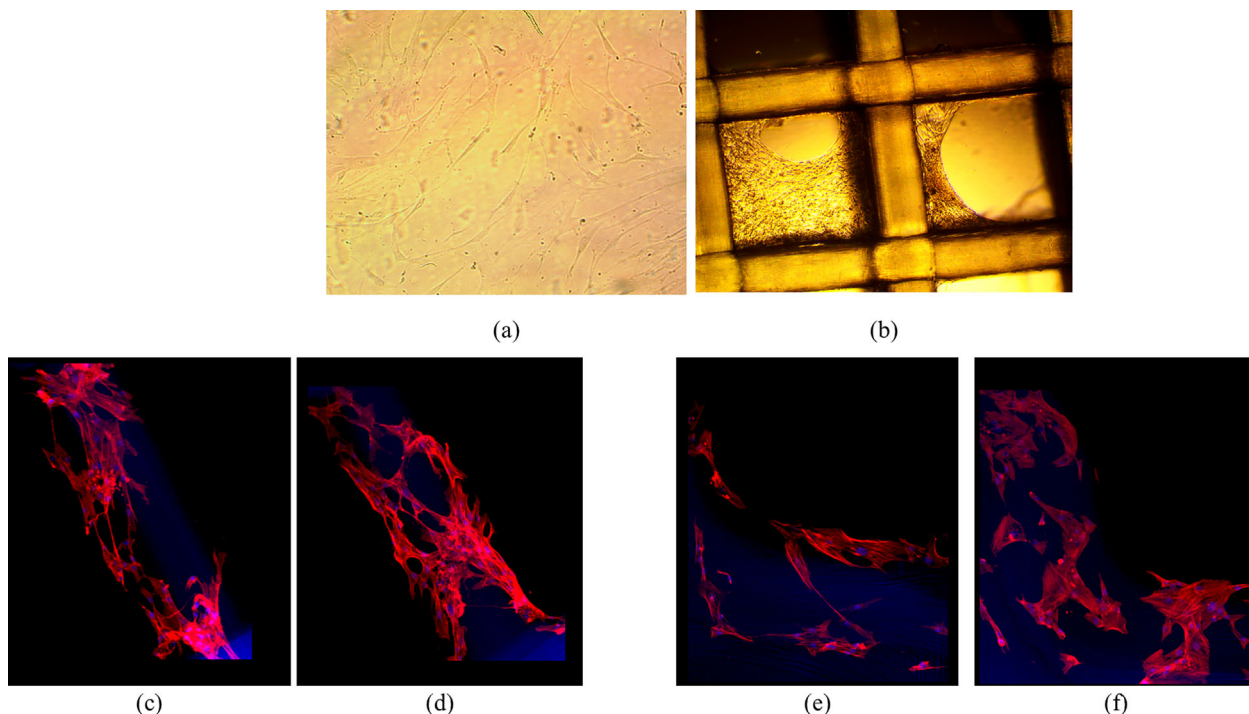

FIGURE 8 Optical microscopy images of hMSC growing on (a) non-porous PEGDA scaffolds after 10 days of culture, (b) porous scaffolds with square geometry after 4 days of culture without LIPUS treatment. Confocal microscopy images of hMSC growth on 3D printed PEGDA scaffolds with square pore geometry (c) before and (d) after 3-day LIPUS stimulation, with hexagonal pore geometry (e) before and (f) after 3-day LIPUS stimulation. The cytoskeleton and cell nuclei were stained by Texas Red®-X phalloidin (red) and DAPI (blue), respectively
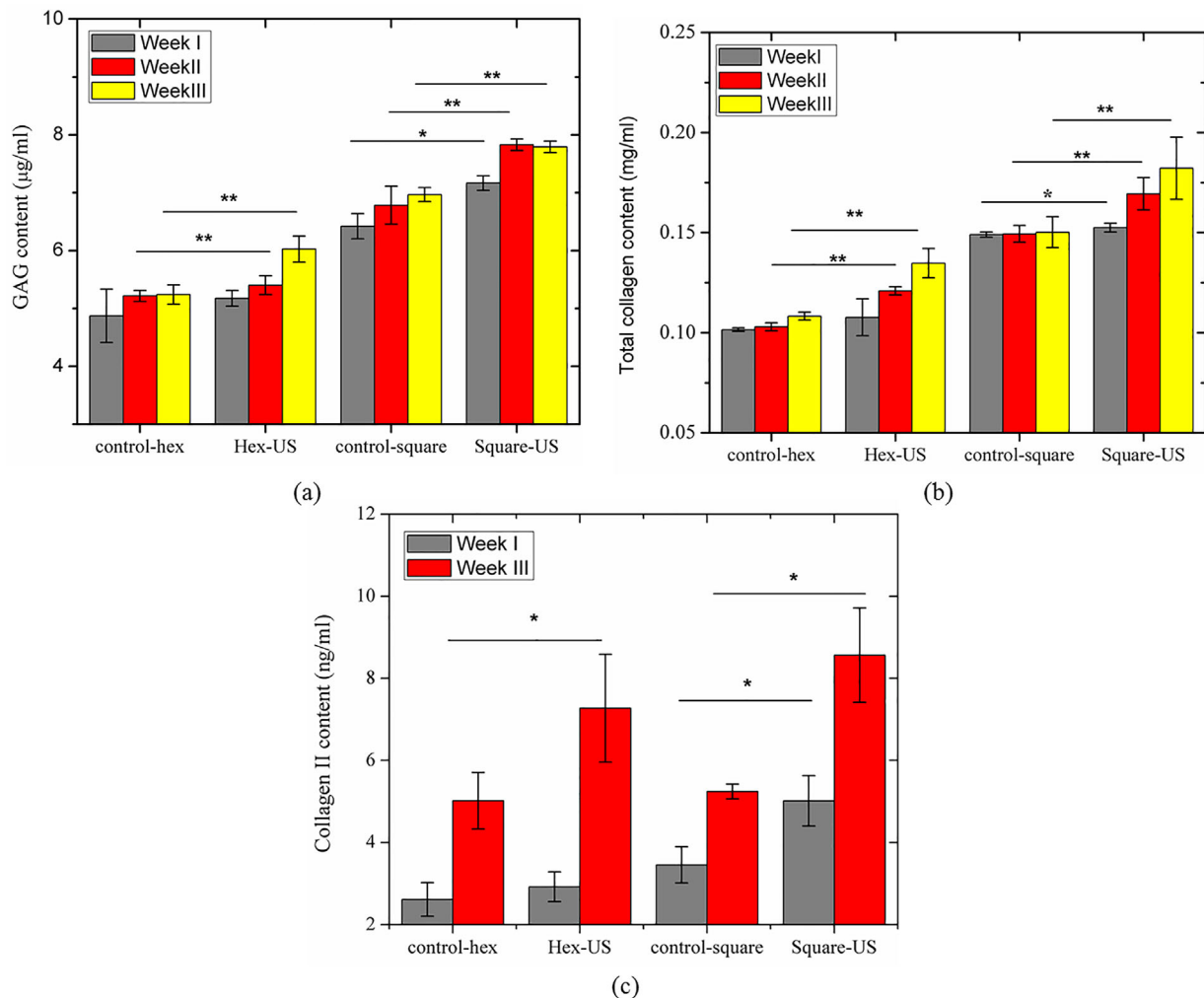
FIGURE 9 Effects of LIPUS (100 mW/cm2; 1.5 MHz; 20% duty cycle; 200 μs pulse length) on synthesis of a) GAG, b) total collagen and c) type II collagen (Data are mean ± StdEM, $n = 5$). Values significantly different from the control group are indicated by * for $p < 0.05$ and ** for $p < 0.01$

Hunziker, 1995; Kim, Sah, Grodzinsky, Plaas, & Sandy, 1994; Smith et al., 1995), LIPUS subjects the cells to a periodically varying load. It is noteworthy to mention that cellular effects of LIPUS are generally categorized to be non-thermal (Dyson, 1982), predominantly due to cavitation, streaming and acoustic radiation forces (Tang, Guha, & Tomé, 2015; Wu & Nyborg, 2008). For the experiments performed here, at less than 200 mW/cm^2, thermal effects are minimal (Claes & Willie, 2007). Duarte (1983) reported negligible temperature variations (∼0.01°C) when LIPUS was used. Because of the low intensities and thereby low mechanical indices (0.05 at 30 mW/cm^2 to 0.12 at 200 mW/cm^2) used in this study, we do not expect strong cavitation activities (Katiyar et al., 2014). Note that reported thresholds for inertial cavitation in water are much higher than parameters studied here (Apfel, 1970; Hill, 1972; Neppiras, 1965). In the absence of thermal and cavitational effects at this acoustic setting, the observed bioeffects most likely arise from the periodic normal stresses as well as shear stresses due to acoustic streaming(Dunn, 1985; Starritt, Duck, & Humphrey, 1989; ter Haar, 1987).

4 | CONCLUSION

We investigated the possibility of using low intensity pulsed ultrasound as an effective tool towards cartilage tissue regeneration in a 3D printed scaffold. We found that hMSCs grow well on porous PEG-DA scaffolds with both hexagonal and square pore shapes when compared to the nonporous ones. Scaffolds with square pores performed better in both cell growth and chondrogenesis than those with hexagonal pores.

We found that LIPUS stimulation promotes hMSC growth and chondrogenic differentiation. The hMSC proliferation enhanced up to 60% 24 hr after LIPUS stimulation. In addition, key cartilage biomarkers such as GAG and type II collagen syntheses showed a significant increase after LIPUS stimulation under optimized acoustic parameters: GAG production increased by 16% in scaffolds with square channels and 11% with hexagonal channels; collagen II production increased by 60% in square and 40% in hexagonal pores. The present investigation suggests that LIPUS, which is non-invasive,

efficient and cost-effective, combined with 3D-printing techniques can be an invaluable tool for cartilage tissue engineering using hMSCs to regenerate damaged cartilages.

ACKNOWLEDGMENTS

ORCID

Mitra Aliabouzar http://orcid.org/0000-0002-2263-7278

REFERENCES

Aliabouzar, M, Zhang, LG, & Sarkar, K. (2016). Lipid coated microbubbles and low intensity pulsed ultrasound enhance chondrogenesis of human mesenchymal stem cells in 3d printed scaffolds. *Scientific Reports*, 6, 37728.

Andersson G . (2008). The burden of musculoskeletal diseases in the United States: Prevalence, societal and economic cost: Amer Academy of Orthopaedic.

Apfel, RE. (1970). The role of impurities in cavitation-threshold determination. *The Journal of the Acoustical Society of America*, 48, 1179–1186.

Athanasiou, KA, Darling, EM, & Hu, JC (2009). Articular cartilage tissue engineering. *Synthesis Lectures on Tissue Engineering*, 1, 1–182.

Azuma, Y, Ito, M, Harada, Y, Takagi, H, Ohta, T, & Jingushi, S. (2001). Low-Intensity pulsed ultrasound accelerates rat femoral fracture healing by acting on the various cellular reactions in the fracture callus. *Journal of Bone and Mineral Research*, 16, 671–680.

Buckwalter, J, & Mankin, H. (1997). Articular cartilage: Degeneration and osteoarthritis, repair, regeneration, and transplantation. *Instructional Course Lectures*, 47, 487–504.

Buschmann, MD, Gluzband, YA, Grodzinsky, AJ, & Hunziker, EB. (1995). Mechanical compression modulates matrix biosynthesis in chondrocyte/agarose culture. *Journal of cell Science*, 108, 1497–1508.

Castro, NJ, O'Brien, J, & Zhang, LG. (2015). Integrating biologically inspired nanomaterials and table-top stereolithography for 3D printed biomimetic osteochondral scaffolds. *Nanoscale*, 7, 14010–14022.

Castro, NJ, Patel, R, & Zhang, LG. (2015). Design of a novel 3D printed bioactive nanocomposite scaffold for improved osteochondral regeneration. *Cellular and Molecular Bioengineering*, 8, 416–432.

Choi, BH, Woo, JI, Min, BH, & Park, SR. (2006). Low-intensity ultrasound stimulates the viability and matrix gene expression of human articular chondrocytes in alginate bead culture. *Journal of Biomedical Materials Research Part A*, 79, 858–864.

Claes, L, & Willie, B. (2007). The enhancement of bone regeneration by ultrasound. *Progress in Biophysics and Molecular Biology*, 93, 384–398.

Clair, BL, Johnson, AR, & Howard, T. (2009). Cartilage repair: Current and emerging options in treatment. *Foot & Ankle Specialist*.

Cui, JH, Park, K, Park, SR, & Min, B-H (2006). Effects of low-intensity ultrasound on chondrogenic differentiation of mesenchymal stem cells embedded in polyglycolic acid: An in vivo study. *Tissue Engineering*, 12, 75–82.

Cui, JH, Park, SR, Park, K, Choi, BH, & Min, B-h (2007). Preconditioning of mesenchymal stem cells with low-intensity ultrasound for cartilage formation in vivo. *Tissue Engineering*, 13, 351–360.

Doan, N, Reher, P, Meghji, S, & Harris, M. (1999). In vitro effects of therapeutic ultrasound on cell proliferation, protein synthesis, and cytokine production by human fibroblasts, osteoblasts, and monocytes. *Journal of Oral and Maxillofacial Surgery*, 57, 409–419.

Duarte, L. (1983). The stimulation of bone growth by ultrasound. *Archives of Orthopaedic and Trauma Surgery*, 101, 153–159.

Dunn, F. (1985). Cellular inactivation by heat and shear. *Radiation and Environmental Biophysics*, 24, 131–139.

Dyson, M. (1982). Non-thermal cellular effects of ultrasound. *The British Journal of Cancer. Supplement*, 5, 165.

Ebisawa, K, Hata, K-i, Okada, K, Kimata, K, Ueda, M, Torii, S, & Watanabe, H. (2004). Ultrasound enhances transforming growth factor β-mediated chondrocyte differentiation of human mesenchymal stem cells. *Tissue Engineering*, 10, 921–929.

Finger, F, Schörle, C, Soder, S, Zien, A, Goldring, MB, & Aigner, T. (2004). Phenotypic characterization of human chondrocyte cell line C-20/A4: a comparison between monolayer and alginate suspension culture. *Cells Tissues Organs*, 178, 65–77.

Gebauer, D, Mayr, E, Orthner, E, & Ryaby, JP. (2005). Low-intensity pulsed ultrasound: Effects on nonunions. *Ultrasound in Medicine & Biology*, 31, 1391–1402.

Grodzinsky, AJ, Levenston, ME, Jin, M, & Frank, EH. (2000). Cartilage tissue remodeling in response to mechanical forces. *Annual Review of Biomedical Engineering*, 2, 691–713.

Habibovic, P, Yuan, H, van der Valk, CM, Meijer, G, van Blitterswijk, CA, & de Groot, K. (2005). 3D microenvironment as essential element for osteoinduction by biomaterials. *Biomaterials*, 26, 3565–3575.

Harle, J, Salih, V, Mayia, F, Knowles, JC, & Olsen, I. (2001). Effects of ultrasound on the growth and function of bone and periodontal ligament cells in vitro. *Ultrasound in Medicine & Biology*, 27, 579–586.

Heckman, JD, Ryaby, JP, McCabe, J, Frey, JJ, & Kilcoyne, RF. (1994). Acceleration of tibial fracture-healing by non-invasive, low-intensity pulsed ultrasound. *The Journal of Bone & Joint Surgery*, 76, 26–34.

Hensel, K, Mienkina, MP, & Schmitz, G. (2011). Analysis of ultrasound fields in cell culture wells for in vitro ultrasound therapy experiments. *Ultrasound in Medicine & Biology*, 37, 2105–2115.

Hill, C. (1972). Ultrasonic exposure thresholds for changes in cells and tissues. *The Journal of the Acoustical Society of America*, 52, 667–672.

Hollander, A, Pidoux, I, Reiner, A, Rorabeck, C, Bourne, R, & Poole, AR. (1995). Damage to type II collagen in aging and osteoarthritis starts at the articular surface, originates around chondrocytes, and extends into the cartilage with progressive degeneration. *Journal of Clinical Investigation*, 96, 2859.

Holmes, B, Castro, NJ, Li, J, Keidar, M, & Zhang, LG. (2013). Enhanced human bone marrow mesenchymal stem cell functions in novel 3D cartilage scaffolds with hydrogen treated multi-walled carbon nanotubes. *Nanotechnology*, 24, 365102.

Holmes, B, Zhu, W, Li, J, Lee, JD, & Zhang, LG. (2014). Development of novel three-dimensional printed scaffolds for osteochondral regeneration. *Tissue Engineering Part A*, 21, 403–415.

Hsu, S-h, Kuo, C-C, Whu, SW, Lin, C-H, & Tsai, C-L (2006). The effect of ultrasound stimulation versus bioreactors on neocartilage formation in tissue engineering scaffolds seeded with human chondrocytes in vitro. *Biomolecular Engineering*, 23, 259–264.

Hunger, PM, Donius, AE, & Wegst, UG. (2013). Structure-property-processing correlations in freeze-cast composite scaffolds. *Acta Biomaterialia*, 9, 6338–6348.

Jin, Q, Takita, H, Kohgo, T, Atsumi, K, Itoh, H, & Kuboki, Y. (2000). Effects of geometry of hydroxyapatite as a cell substratum in BMP-induced ectopic bone formation. *Journal of Biomedical Materials Research*, 51, 491–499.

Johnstone, B, Hering, TM, Caplan, AI, Goldberg, VM, & Yoo, JU. (1998). In vitrochondrogenesis of bone marrow-derived mesenchymal progenitor cells. *Experimental Cell Research*, 238, 265–272.

Kassem, M. (2004). Mesenchymal stem cells: Biological characteristics and potential clinical applications. *Cloning and Stem Cells*, 6, 369–374.

Katiyar, A, Duncan, RL, & Sarkar, K. (2014). Ultrasound stimulation increases proliferation of MC3T3-E1 preosteoblast-like cells. *Journal of Therapeutic Ultrasound*, 2, 1.

Kim, Y-J., Grodzinsky, AJ, & Plaas, AH. (1996). Compression of cartilage results in differential effects on biosynthetic pathways for aggrecan, link protein, and hyaluronan. *Archives of Biochemistry and Biophysics*, 328, 331–340.

Kim, Y-J., Sah, RL, Grodzinsky, AJ, Plaas, AH, & Sandy, JD. (1994). Mechanical regulation of cartilage biosynthetic behavior: Physical stimuli. *Archives of Biochemistry and Biophysics*, 311, 1–12.

Knychala, J, Bouropoulos, N, Catt, C, Katsamenis, O, Please, C, & Sengers, B. (2013). Pore geometry regulates early stage human bone marrow cell tissue formation and organisation. *Annals of Biomedical Engineering*, 41, 917–930.

Korstjens, C, Van der Rijt, R, Albers, G, Semeins, C, & Klein-Nulend, J. (2008). Low-intensity pulsed ultrasound affects human articular chondrocytes in vitro. *Medical & Biological Engineering & Computing*, 46, 1263–1270.

Kumar, A, Mollah, AA, Keshri, AK, Kumar, M, Singh, K, Rallabhandi, KDVS, & Seelaboyina, R. (2016). Development of macroporous silicone rubber for acoustic applications. *Industrial & Engineering Chemistry Research*, 55, 8751–8760.

Kuo, CK, Li, W-J., Mauck, RL, & Tuan, RS. (2006). Cartilage tissue engineering: Its potential and uses. *Current Opinion in Rheumatology*, 18, 64–73.

Lai, C-H., Chen, S-C., Chiu, L-H., Yang, C-B., Tsai, Y-H., Zuo, CS, . . . Lai, W-F. (2010). Effects of low-intensity pulsed ultrasound, dexamethasone/TGF-β1 and/or BMP-2 on the transcriptional expression of genes in human mesenchymal stem cells: Chondrogenic vs. osteogenic differentiation. *Ultrasound in Medicine & Biology*, 36, 1022–1033.

Lawrence, RC, Felson, DT, Helmick, CG, Arnold, LM, Choi, H, Deyo, RA, . . . Hunder, GG. (2008). Estimates of the prevalence of arthritis and other rheumatic conditions in the United States: Part II. *Arthritis & Rheumatism*, 58, 26–35.

Li, JG-R., Chang, WH-S., Lin, JC-A., & Sun, J-S. (2002). Optimum intensities of ultrasound for PGE 2 secretion and growth of osteoblasts. *Ultrasound in Medicine & Biology*, 28, 683–690.

Loh, QL, & Choong, C. (2013). Three-dimensional scaffolds for tissue engineering applications: Role of porosity and pore size. *Tissue Engineering Part B: Reviews*, 19, 485–502.

Matthews, BD, Overby, DR, Mannix, R, & Ingber, DE. (2006). Cellular adaptation to mechanical stress: Role of integrins, Rho, cytoskeletal tension and mechanosensitive ion channels. *Journal of Cell Science*, 119, 508–518.

Mayr, E, Frankel, V, & Rüter, A. (2000). Ultrasound-an alternative healing method for nonunions? *Archives of Orthopaedic and Trauma Surgery*, 120, 1–8.

Mukai, S, Ito, H, Nakagawa, Y, Akiyama, H, Miyamoto, M, & Nakamura, T. (2005). Transforming growth factor-β 1 mediates the effects of low-intensity pulsed ultrasound in chondrocytes. *Ultrasound in Medicine & Biology*, 31, 1713–1721.

Munevar, S, Wang, Y-l, & Dembo, M. (2004). Regulation of mechanical interactions between fibroblasts and the substratum by stretch-activated Ca2+ entry. *Journal of Cell Science*, 117, 85–92.

Nelson, CM, Jean, RP, Tan, JL, Liu, WF, Sniadecki, NJ, Spector, AA, & Chen, CS. (2005). Emergent patterns of growth controlled by multicellular form and mechanics. *Proceedings of the National Academy of Sciences of the United States of America*, 102, 11594–11599.

Neppiras, E. (1965). Measurements in liquids at medium and high ultrasonic intensities. *Ultrasonics*, 3, 9–17.

Nishikori, T, Ochi, M, Uchio, Y, Maniwa, S, Kataoka, H, Kawasaki, K, . . . Kuriwaka, M. (2002). Effects of low-intensity pulsed ultrasound on proliferation and chondroitin sulfate synthesis of cultured chondrocytes embedded in Atelocollagen® gel. *Journal of Biomedical Materials Research*, 59, 201–206.

O'Brien, CM, Holmes, B, Faucett, S, & Zhang, LG. (2014). Three-dimensional printing of nanomaterial scaffolds for complex tissue regeneration. *Tissue Engineering Part B: Reviews*, 21, 103–114.

Olympus N. Ultrasonic transducers technical notes. Technical brochure: Olympus NDT, Waltham, MA 2006; 2:2.2.

Parvizi, J, Wu, CC, Lewallen, DG, Greenleaf, JF, & Bolander, ME. (1999). Low-intensity ultrasound stimulates proteoglycan synthesis in rat chondrocytes by increasing aggrecan gene expression. *Journal of Orthopaedic Research*, 17, 488–494.

Pittenger, MF, Mackay, AM, Beck, SC, Jaiswal, RK, Douglas, R, Mosca, JD, . . . Marshak, DR. (1999). Multilineage potential of adult human mesenchymal stem cells. *Science*, 284, 143–147.

Responte, DJ, Natoli, RM, & Athanasiou, KA. (2007). Collagens of articular cartilage: Structure, function, and importance in tissue engineering. *Critical Reviews™ in Biomedical Engineering*, 35.

Rumpler, M, Woesz, A, Dunlop, JW, van Dongen, JT, & Fratzl, P. (2008). The effect of geometry on three-dimensional tissue growth. *Journal of the Royal Society Interface*, 5, 1173–1180.

Saito, M, Fujii, K, Tanaka, T, & Soshi, S. (2004). Effect of low-and high-intensity pulsed ultrasound on collagen post-translational modifications in MC3T3-E1 osteoblasts. *Calcified Tissue International*, 75, 384–395.

Sims, JR, Karp, S, & Ingber, DE. (1992). Altering the cellular mechanical force balance results in integrated changes in cell, cytoskeletal and nuclear shape. *Journal of Cell Science*, 103, 1215–1222.

Smith, RL, Donlon, B, Gupta, M, Mohtai, M, Das, P, Carter, D, & Schurman, D. (1995). Effects of fluid-induced shear on articular chondrocyte morphology and metabolism in vitro. *Journal of Orthopaedic Research*, 13, 824–831.

Sobral, JM, Caridade, SG, Sousa, RA, Mano, JF, & Reis, RL. (2011). Three-dimensional plotted scaffolds with controlled pore size gradients: Effect of scaffold geometry on mechanical performance and cell seeding efficiency. *Acta Biomaterialia*, 7, 1009–1018.

Starritt, H, Duck, F, & Humphrey, V. (1989). An experimental investigation of streaming in pulsed diagnostic ultrasound beams. *Ultrasound in Medicine & Biology*, 15, 363–373.

Suzuki, A, Takayama, T, Suzuki, N, Sato, M, Fukuda, T, & Ito, K. (2009). Daily low-intensity pulsed ultrasound-mediated osteogenic differentiation in rat osteoblasts. *Acta Biochimica Et Biophysica Sinica*, 41, 108–115.

Takayama, T, Suzuki, N, Ikeda, K, Shimada, T, Suzuki, A, Maeno, M, . . . Ito, K. (2007). Low-intensity pulsed ultrasound stimulates osteogenic differentiation in ROS 17/2.8 cells. *Life Sciences*, 80, 965–971.

Tang, J, Guha, C, & Tomé, WA. (2015). Biological effects induced by non-thermal ultrasound and implications for cancer therapy a review of the current literature. *Technology in Cancer Research & Treatment*, 14, 221–235.

Temenoff, JS, & Mikos, AG (2000). Review: Tissue engineering for regeneration of articular cartilage. *Biomaterials*, 21, 431–440.

ter Haar, G (1987). *Interaction mechanisms: Non-thermal, non-cavitational effects*. Ultrasound, Springer, (pp. 105–116).

Williams, AR. (1983). *Ultrasound: Biological effects and potential hazards*. London (UK): Academic Press, (p. 1983).

Wu, J, & Nyborg, WL. (2008). Ultrasound, cavitation bubbles and their interaction with cells. *Advanced Drug Delivery Reviews*, 60, 1103–1116.

Zeltinger, J, Sherwood, JK, Graham, DA, Müeller, R, & Griffith, LG. (2001). Effect of pore size and void fraction on cellular adhesion, proliferation, and matrix deposition. *Tissue Engineering*, 7, 557–572.

Zhang, L, Hu, J, & Athanasiou, KA. (2009). The role of tissue engineering in articular cartilage repair and regeneration. *Critical Reviews in Biomedical Engineering*, 37, 1–57.

Zhang, Z-J., Huckle, J, Francomano, CA, & Spencer, RG. (2003). The effects of pulsed low-intensity ultrasound on chondrocyte viability, proliferation, gene expression and matrix production. *Ultrasound in Medicine & Biology*, 29, 1645–1651.

Zhou, X, Castro, NJ, Zhu, W, Cui, H, Aliabouzar, M, Sarkar, K, & Zhang, LG. (2016). Improved human bone marrow mesenchymal stem cell osteogenesis in 3D bioprinted tissue scaffolds with low intensity pulsed ultrasound stimulation. *Scientific Reports*, *6*, 32876.

Zhou, X, Nowicki, M, Cui, H, Zhu, W, Fang, X, Miao, S, . . . Zhang, LG. (2017). 3D bioprinted graphene oxide-incorporated matrix for promoting chondrogenic differentiation of human bone marrow mesenchymal stem cells. *Carbon*, *116*, 615–624.

Zhou, X, Zhu, W, Nowicki, M, Miao, S, Cui, H, Holmes, B, . . . Zhang, LG. (2016). 3D bioprinting a cell-Laden bone matrix for Breast cancer metastasis study. *ACS Applied Materials & Interfaces*, *8*, 30017–30026.

Zhu, W, Holmes, B, Glazer, RI, & Zhang, LG. (2016). 3D printed nanocomposite matrix for the study of breast cancer bone metastasis. Nanomedicine: Nanotechnology. *Biology and Medicine*, *12*, 69–79.

Zhu, W, O'Brien, C, O'Brien, JR, & Zhang, LG (2014). 3D nano/microfabrication techniques and nanobiomaterials for neural tissue regeneration. *Nanomedicine*, *9*, 859–875.